Near Ultraviolet Photostability of Liquid Crystal Mixtures

Anna M. Lackner [a] , J. David Margerum [a] & Camille Van Ast [a]

[a] Hughes Research Laboratories, 3011 Malibu Canyon Road, Malibu, California, 90265, USA

PLEASE SCROLL DOWN FOR ARTICLE

Near Ultraviolet Photostability of Liquid Crystal Mixtures

ANNA M. LACKNER, J. DAVID MARGERUM, and CAMILLE VAN AST

Hughes Research Laboratories, 3011 Malibu Canyon Road, Malibu, California 90265, USA

Liquid crystal material photostability was investigated for application in high intensity projectors operating with both near ultraviolet (UV) and visible light. Commercially available mixtures were studied in transparent test cells and their lifetimes were correlated with their chemical structures. Substantial improvements were observed in the photostability of hybrid field effect cells by using pure nematic mixtures whose major components had one or two cyclohexyl groups in place of phenyl groups. However, overriding the importance of these structural effects, polar impurities present in some of the nematic mixtures with cyclohexane groups caused a large decrease in photostability.

Results were obtained by examining the photostability of eight different commercial liquid crystal mixtures, with highly positive dielectric anisotropy, whose components include a variety of structural types. Although the resistivity of each liquid crystal mixture decreased steadily with exposure, the reported end of life corresponded to the first observable change in the liquid crystal alignment toward a higher off-surface tilt. Near-UV/visible exposures (356-790 nm band) from a 900 W xenon lamp resulted in lifetimes of 3800 h for ZLI-1800 and 800 h for ZLI-1132 compared to only 230 h for a BDH-E7 cell.

Keywords: photostability, liquid crystal mixtures, light valves, hybrid field effect, impurities, cyclohexane rings.

I. INTRODUCTION

Liquid crystal (LC) materials with acceptable operational lifetime are needed for high intensity projectors in the near UV and visible region. In this study, we determined the feasibility of using other commercially available LC mixtures in place of BDH-E7. LC mixtures with structural configurations expected to be more stable were selected
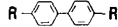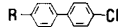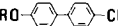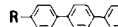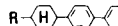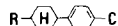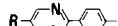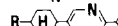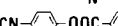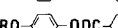
and evaluated for performance lifetime under accelerated test conditions with broad band UV/visible light. In general, LC mixtures containing a higher percentage of saturated components, with lower absorption in the UV, were more stable. However, the polar impurities present in some of the commercial LC samples were the controlling factor in their decomposition rate, even with predominately phenylcyclohexane LC components. In this paper we show how the effect of such impurities on photostability was determined by separating impurities from the major components of the LC, analyzing them, and redoping them back into a pure mixture. The lifetime was greatly extended by removing the impurity and shortened by redoping it back into a LC sample. Finally we show that pure mixtures with saturated components have lifetimes of more than an order of magnitude longer than that of BDH-E7.

II. EXPERIMENTAL

This study includes measurements on seven commercial liquid crystal mixtures selected as potential candidates for near-UV applications, and for comparisons with BDH-E7. Table I summarizes their composition and properties as compared with BDH-E7, which was previously used in the Hughes liquid crystal light valve (LCLV). These mixtures were chosen primarily because they were expected to show less UV and blue light absorption than BDH-E7. Most of them contain structures with some cyclohexyl groups used in place of phenyl groups. Because some Hoffmann LaRoche samples (RO-TN-619 and RO-TN-653) contain pyrimidine components as well, we also chose to study their RO-TN-2025 in these comparisons; it contains only pyrimidine and biphenyl components. The variety of structures represented by the components of these seven LC mixtures was expected to be helpful in estimating qualitative comparisons of photostability for different structural groups. Transparent test cells of 6.4 μm nominal spacing were made by the Hughes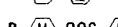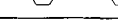 Industrial Products Division for each of the eight LCs. These cells had electrodes of 500 Å indium tin oxide (ITO) overcoated with straight sputtered SiO_2 (2000 Å) for insulation, and had angle deposited SiO_2 for alignment. The cells were filled by our standard LCLV technology using normal O-ring seals in the cell holder. Hybrid field effect response curves were obtained for each cell in reflection (using external mirrors) at several wavelengths by using interference filters in the incident light beam. Typical results for BDH-E7 and ZLI-1800 are shown in Figures 1 and 2.

TABLE I

Composition and physical properties of liquid crystal mixtures chosen for near UV
photostability studies

CLASS STRUCTURE	BDH-E7	MERCK 1132	RO-TN-619	MERCK 1083	MERCK 1738	MERCK 1800	RO-TN-653	RO-TN-2025
WEIGHT % IN MIXTURE								
R-◇-◇-R			15					
R-◇-◇-CN	77		17		√			69
RO-◇-◇-CN	15							
R-◇-◇-◇-CN	8				√			
R-(H)-◇-◇-CN		15			√			
R-(H)-◇-CN		85		100	√	√		
R-(H)-(H)-CN						√		
R-⟨N=N⟩-◇-CN / R-(H)-⟨N=N⟩-◇-CN			7				28	31
CN-◇-OOC-◇-R							6	
RO-◇-OOC-(H)-R / CN-◇-OOC-(H)-R			61			√	66	
R-(H)-◇-OOC-(H)-R						√		
R-(H)-OOC-(H)-(H)-R						√		
PHYSICAL PROPERTIES								
NEMATIC PHASE, °C	-10 TO 61	-6 TO 70	<-10 TO 61	-3 TO 51	-6 TO 70	-9 TO 60	<-15 TO 72	<-10 TO 60
VISCOSITY, 20 °C	40	28	27	21	30	29	42	41
DIELECTRIC ANISOTROPY	11.0	10.1	5.8	10.1	13.3	7.0	12.4	17.7
OPTICAL ANISOTROPY	0.225	0.14	0.123	0.12	0.202	0.08	0.134	0.217

The photostability of an LC mixture in the near UV band of light is highly dependent on its spectral absorption in that region. We chose to study the absorption spectra of LCs in solvents, because some light scattering effects are present even in well aligned nematic LCs. We used a relatively high concentration of LC (1–4%) in long path-length cells (5 or 10 cm) to measure absorption tails of components and impurities into the visible range in acetonitrile or hexane solvents, as shown in Figures 3 through 5. The extinction coefficient used here is defined as $\epsilon_w = A/lc_w$, where A is the absorbance (optical density). l is the path length in cm, and c_w is the mass of LC (in grams) per 100 ml of solution. This coefficient shows the relative absorbance of the LC mixtures in an isotropic solution. Although both anisotropic
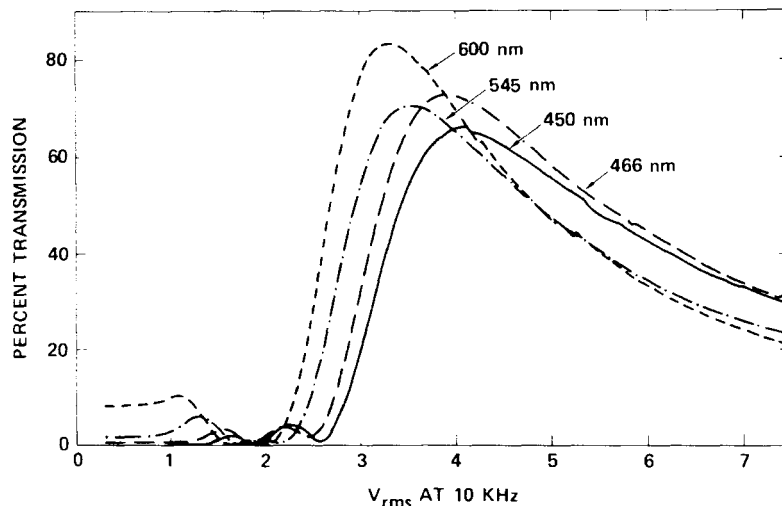
FIGURE 1   Hybrid field effect curves of Merck-1132 LC.

and intermolecular effects will alter the spectra of 100% LC mixtures, these coefficients give an approximate indication of the expected LC absorption. For example, if ϵ_w = 1.0 for an LC with a density of 1.0, then a 10 μm pathlength will have A = 0.001, or T = 99.8%.

The spectral distribution of our lamp exposure system[1] used for the photostability rating of all eight LC mixtures, consisted of a 900
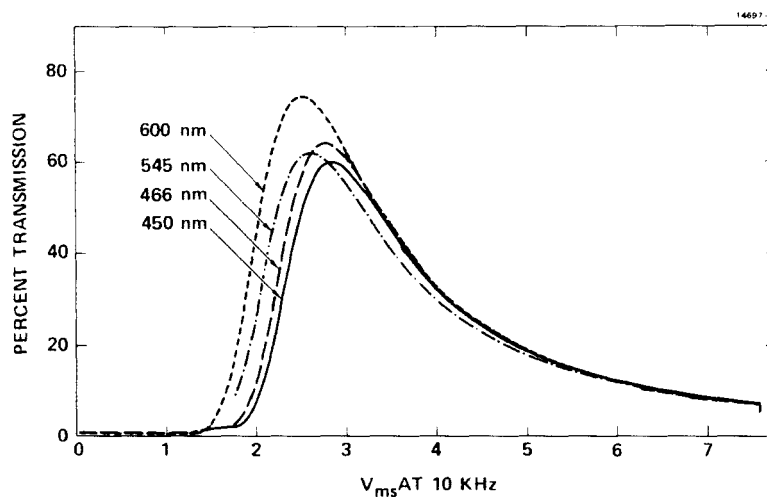
FIGURE 2   Hybrid field effect curves of Merck-1800 LC.
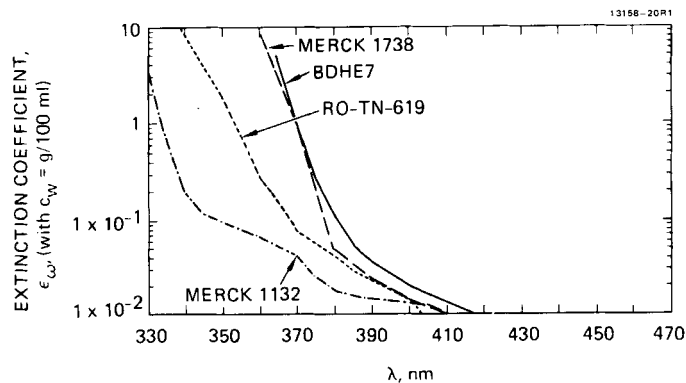
FIGURE 3 Solution spectra of liquid crystals in acetonitrile.

W lamp (Xenolite CXL-900 ozone-free, xenon short arc lamp) with a lens system, a 6 in. water cell filter (pyrex windows) and the nominal $\lambda > 356$ nm filter system. Typical light intensities were about 500 mW/cm^2 with the spectral distribution shown in Figure 6. The nominal $\lambda > 356$ filter combination, with 1% transmission cut-off at 356 nm, contained Corning CS 0-52, and CS 1-75 filters, and a 360 nm hot mirror. Exposure tests of the LC cells were made with an external mirror attached to the rear window, to give a double pass exposure of the light beam.

Several techniques were used to observe photodegradation of the LC cells. With the optical system used, which gave a high intensity

FIGURE 4 Solution spectra of liquid crystals in acetonitrile.

FIGURE 5   Solution spectra of liquid crystals.

FIGURE 6   Spectral distribution of light used for photostability exposures.

"hot" spot in the center area of the cell, the techniques were most useful in the following order:

- Visual observation of LC off-parallel surface tilt (in the center of the cell, compared to the surrounding area) by viewing the cell through crossed polarizers and noting differences in the birefringence colors. This method was used to denote end of life.
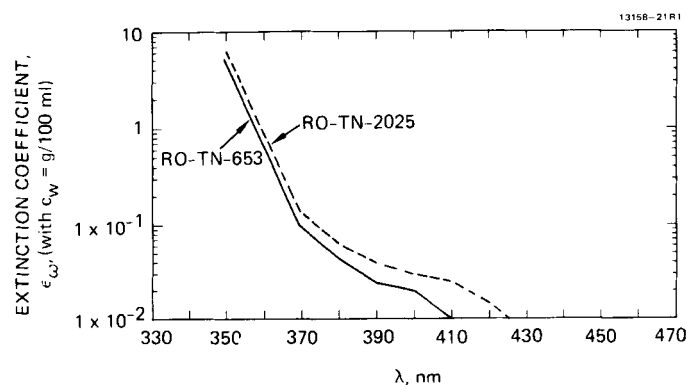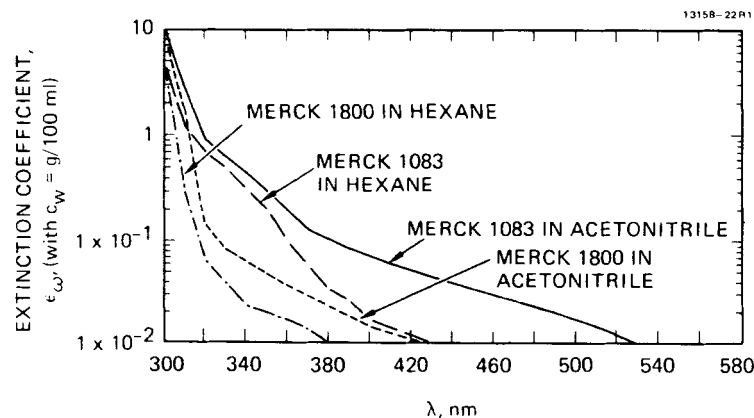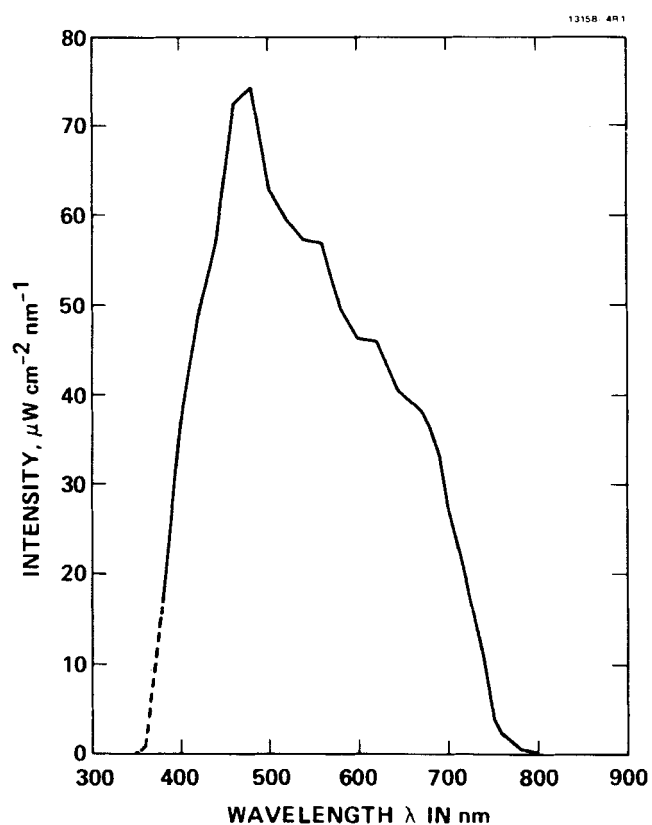
- Change of the hybrid field effect electro-optical response curves. This was the method that we previously used to estimate cell failure.[1] However, because our optical analysis beam was larger than the high intensity hot spot, this generally showed end of life later than the visual inspection of alignment tilt in the hot spot area.

- Polarized light spectrophotometer curves of transmission vs. wavelength were used for apparent thickness determination by the interference pattern technique. Using the extraordinary index (n_e), the calculated cell thickness changed from the initial (actual) value to a smaller apparent thickness as exposure caused surface tilt of the LC. The sensitivity of the change in the apparent cell thickness depends on the size of the optical beam used in the spectrophotometer compared to the hot spot area; this method was not as sensitive· as the visual method.

- Change in apparent cell LC resistivity. Most of the cells failed when their $\rho_{apparent}$ dropped below about 2×10^{10} Ω-cm. Although this was not a very sensitive indication of photodegradation failure, it was used to predict the approximate lifetime (prior to completion of exposure) of cells filled with these LCs.

The liquid crystal samples were all analyzed by high performance liquid chromatography (HPLC) and by gas chromatography (GC), and one sample was purified by preparative liquid chromatography. HPLC runs were made with the Model 6000 solvent delivery system from Waters Associates, with a 250 μl injection loop using a Microporasil column and a Waters Model 440 dual-channel UV absorption detector. Both channels used 254 nm, with one set at 2.0 absorption units full scale (AUFS) and the other at 0.02 AUFS, to give different ranges of light absorption sensitivity. Figure 7 shows the result of a batch of Merck-1132 eluted by the solvent system "19:4:1," which refers to the volume ratios of hexane/chloroform/acetonitrile in this mixed solvent. Under these conditions the four components all appear together as an off-scale peak, with only one impurity peak shown, which appeared before that of the components.

For GC analysis, the instrumentation used was a Hewlett Packard Model 5730A gas chromatograph with dual columns (6 ft. long, 3%

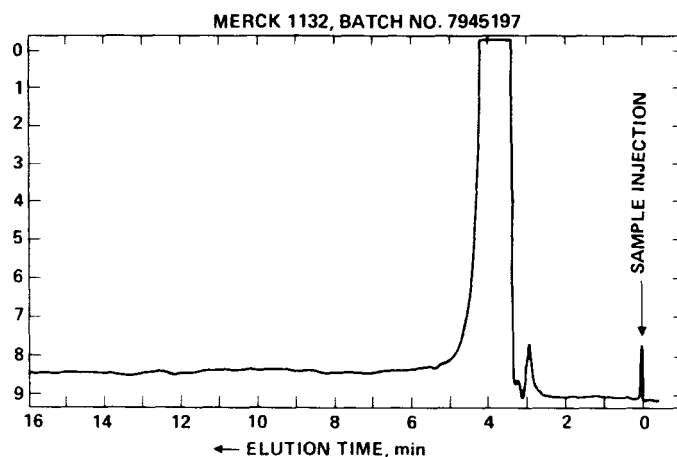FIGURE 7   HPLC trace of Merck-1132 (batch 7945197).

OV-225, 100/120 mesh, Gas Chrom Q, from Applied Science), a flame ionization detector, and nitrogen carrier gas at 45 ml/min. The injection port and detector area temperatures were 300°C. The injected samples were 10% LC in hexane solutions. The component peak positions are shown in Figure 8, where a temperature program
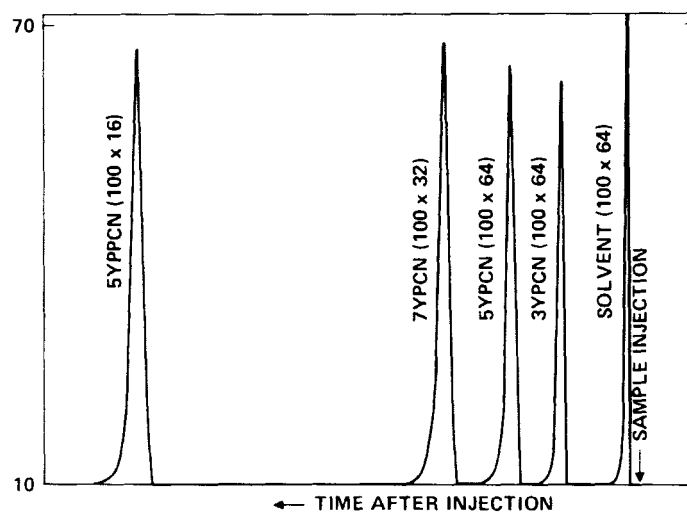

FIGURE 8   GC analysis of Merck-1132.

for the column was 220°C for 2 min., followed by a 4°C/min. increase to 300°C.

When LC mixtures were purified by liquid chromatography, we used the Waters Associates Prep LC/System 500 instrument with one Prep Pak 550 column (silica gel) for the sample. The "19:4:1" solvent system was used, and 3 g samples were processed through the column at a time.

III. RESULTS AND DISCUSSION

Seven commercial LC mixtures representative of various LC structure combinations were chosen and studies were made on their near-UV to visible absorption spectra and relative photo-stability under accelerated conditions. Comparisons were made with BDH-E7 as a reference material.

The as-received LC samples showed the following order for the best transparency (least absorption in solutions) in the two spectral regions indicated:

Near-UV (360 to 400 nm): 1800 > 1132 > 619 > 653 >

$$1738 > 2025 > E7 > 1132\dagger > 1083\dagger$$

UV and VIS (λ > 385 nm): 1800 > 1132 > 653 > 619 >

$$1738 > E7 > 2025 > 1132\dagger > 1083\dagger$$

These sequences indicate the relative absorption of light in the photosensitive region. (The LC photostabilities would have the same sequences as above only if all components of all the mixtures had approximately the same quantum yield of degradation.) As indicated in Figures 3 through 5, all of the other seven LC mixtures absorb less UV light than does BDH-E7, and they have a high absorption cutoff (ϵ_w > 10) at a lower UV wavelength than BDH-E7. However, several of the LCs showed absorption tails in the visible that were higher than that of BDH-E7. Such higher absorption in the visible was particularly prominent for the sample of Merck-1083†. The Merck-1738 sample showed nearly the same absorption as BDH-E7, while

---

† These samples of ZLI-1132 and ZLI-1083 were found to contain substantial amounts of impurities.

Merck-1132 showed about 60% as much absorption as BDH-E7 in the visible range (for batch 794197). The Hoffmann LaRoche samples of RO-TN-619 and RO-TN-653 showed much less visible absorption that BDH-E7, while the absorption of RO-TN-2025 was higher than BDH-E7 in the 390 to 425 nm range, but lower than BDH-E7 above 425 nm. A direct comparison of the extinction coefficients at two wavelengths is given in Table II. A low value of $\epsilon_{LC}/\epsilon_{E7}$ is favorable, while a ratio above unity is unfavorable because it indicates a larger light absorption by the LC studied than for the BDH-E7 sample. The results in Table II are listed in the order of the lowest $\epsilon_{LC}/\epsilon_{E7}$ ratio at 385 nm, with the most favorable sample at the top. Note that while one batch of Merck-1132 is listed at the top of Table II, another batch is listed at the bottom. This second batch of Merck-1132† was worse than any of the other samples at 385 nm because of impurities present in it.

TABLE II

Extinction coefficient comparison in acetonitrile

LC IN CH_3CN	λ, nm	ϵ_w	$\epsilon_{LC}/\epsilon_{E7}$
MERCK 1132 BATCH NO. 7945197	360 385	0.068 0.016	0.007 0.316
MERCK 1800 BATCH NO. R169	360 385	0.037 0.021	0.004 0.402
RO-TN-619 HOFFMAN — LA ROCHE	360 385	0.274 0.029	0.028 0.563
RO-TN-653 HOFFMAN — LA ROCHE	360 385	0.678 0.032	0.068 0.609
MERCK 1738 BATCH NO. 1071154	360 385	8.620 0.034	0.867 0.661
RO-TN-2025 HOFFMAN — LA ROCHE	360 385	0.902 0.049	0.091 0.939
BDH E7 BATCH NO. 508797	360 385	9.940 0.052	1.000 1.000
MERCK 1083 BATCH NO. 8537949	360 385	0.181 0.092	0.018 1.772
MERCK 1132 BATCH NO. 0041861	360 385	0.296 0.107	0.030 2.050

The Merck-1083† sample (and the batch of Merck-1132†) contained impurities which contributed to their absorption above 385 nm. Based on the similarity of their compositions, a pure Merck-1083 sample should have shown less absorption than the good Merck-1132 sample throughout the entire spectral region. Structural comparisons between Merck-1800 and Hoffman LaRoche RO-TN-619 indicate that the higher visible absorption measurement for the Merck-1800 sample in acetonitrile was probably due either to impurities or due to light scattering by insoluble LC particles (or droplets) in this solvent. The solution spectrum of Merck-1800 in hexane showed a much lower visible absorption tail, which was lower than the Merck-1132.

The result of our accelerated lifetests are shown in Figures 9 and 10. End of life is denoted with larger circles, and was determined from visual observation between crossed polarizers of the LC off-

900 W XENON LAMP, 356 nm CUTOFF FILTER (1% T)
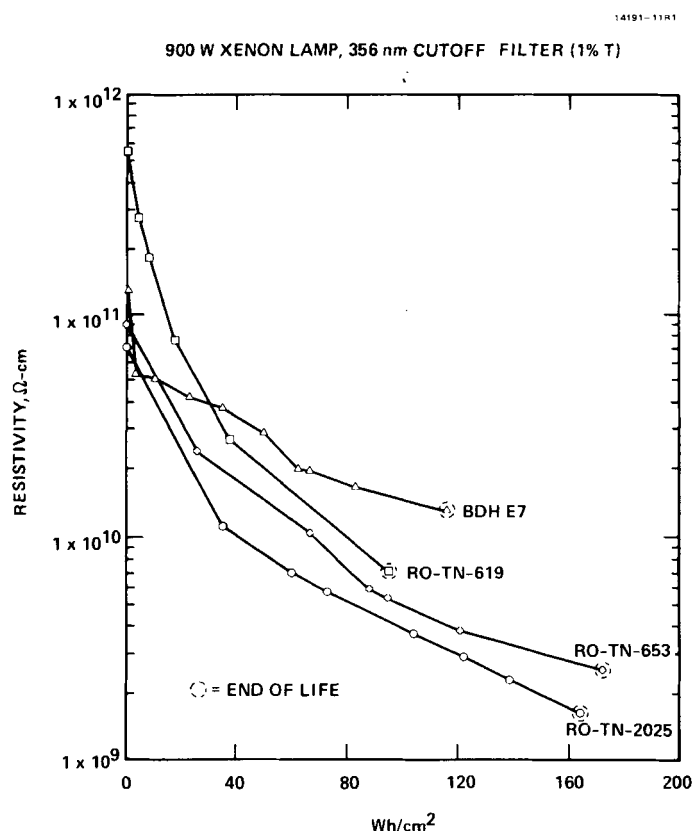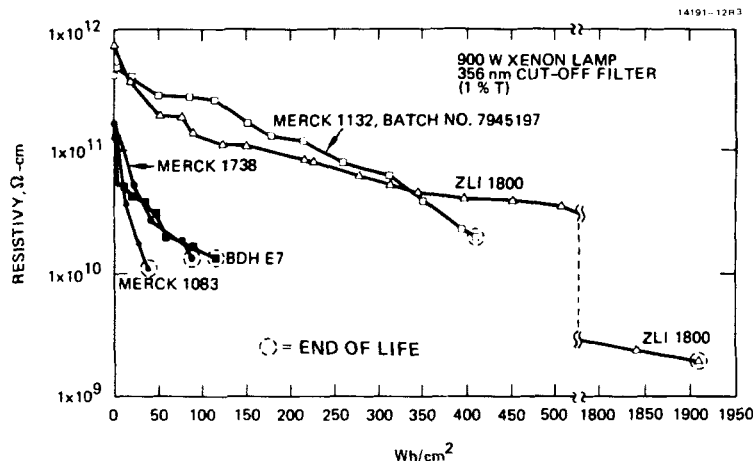
FIGURE 9   Exposure of test cells in LCLV holders.

FIGURE 10   Exposure of test cells in LCLV holders.

parallel surface tilt. The resistivities in Figures 9 and 10 are based on an assumed thickness of 6.4 μm, corresponding to the cell spacers. The actual cell thicknesses are larger (about 8 μm instead of 6 μm) thus the actual LC resistivities are all lower than those shown in Figures 9 and 10. In addition, the SiO_2 overcoatings are responsible for an apparent resistivity of about 1.2×10^9 Ω-cm in these cells, so that the actual LC $\rho_{apparent}$ values of the LCLV are also higher than the actual LC resistivities as a result of the SiO_2. (Corrections for the SiO_2 is significant only for $\rho_{apparent} < 10^{10}$ Ω-cm.) Nevertheless, the $\rho_{apparent}$ resistivities shown in Figures 9 and 10 do seem to be related to the photostability of the LC samples. The samples with lower initial $\rho_{apparent}$ tend to be less photostable and most of LC test cells failed when $\rho_{apparent}$ was in the 6×10^9 to 2×10^{10} Ω-cm range. (The only exceptions were RO-TN-2025 and ZLI-1800, which failed at a $\rho_{apparent}$ of 2×10^9 Ω-cm.)

The photodegradation lifetimes are summarized in Table III. The relative photoinstability of the LC cells was similar to the relative absorption of the UV to visible light by the LCs in solution. It is important to note, however, that the photostability observed in these cells was highly dependent on the presence or absence of impurities and probably also of oxygen. The tremendous effects of impurities are demonstrated by the short exposure life of the impure batch of Merck-1132 when compared with the long exposure life of the purer batch. Impurities are also responsible for the short lifetime of Merck-1083†, and possibly limit the lifetime of other samples as well. Since

TABLE III

Impurities and photodegradation rates of LC mixtures

13158-5R4

LC MIXTURES	BDH-E7	MERCK 1132 (NO. 0041861)	MERCK 1132 (NO. 7945197)	RO-TN-619	MERCK 1083	MERCK 1738	MERCK 1800	RO-TN-653	RO-TN-2025
ABSORPTION COEFFICIENT									
ϵ_ω AT 360 nm	9.94	0.30	0.07	0.27	0.18	8.62	0.04	0.68	0.90
385 nm	0.05	0.11	0.02	0.03	0.09	0.03	0.02	0.03	0.05
TOTAL IMPURITY BY HPLC, %	0.09	1.62	0.03	<0.01	1.78	0.44	0.19	0.09	0.04
RESISTIVITY, Ω-cm	1.3×10^{11}	7.8×10^{10}	3.4×10^{12}	5.3×10^{11}	1.7×10^{11}	1.9×10^{11}	7.3×10^{11}	8.5×10^{10}	6.5×10^{10}
PHOTODEGRADATION STUDIES	IN Wh/cm² (WITH $\lambda > 356$ nm, 0.5 W/cm², O-RING SEALED TEST CELL)								
• CELL LIFE	116	35	412	59	26	89	1909	172	163

we are not sure that all of our O-ring sealed cells are equally effective in their exclusion of oxygen, we are cautious about drawing conclusions about the effect of LC structure on photostability.

The final results with the seven types of commercial LC mixtures in comparison to BDH-E7 indicates the following order of photostability:

$$UV/Blue\ (\lambda > 356\ nm):\ 1800 > 1132 > 653 > 2025 > E7$$

$$> 1738 > 619 > 1132\dagger > 1083^{\dagger}$$
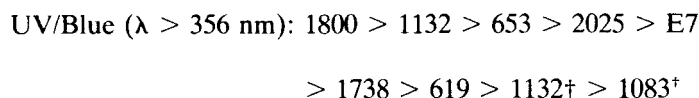
If we assume that the amount of oxygen is constant in these O-ring sealed test cells, this sequence indicates that in this wavelength region ($\lambda > 356$ nm) the LC components are photostable in approximately the order shown in Figure 11 (which includes both molecular absorption and photostability effects).

The rapid degradation observed for Merck-1083† (in just 27 Wh/cm^2) was due to the impurities in this particular sample, since otherwise it would be expected to be more stable than the good Merck-1132 which lasted more than 313 Wh/cm^2. This clearly demonstrated the need to avoid impurities in the LC, whatever the structure of the main components. To indicate the LC mixture purity we chose HPLC and GC analysis. Total impurity by HPLC analysis for all eight LC mixtures, listed in Table III, showed impurity levels above 1% only for Merck-1083† and Merck-1132† (batch 0041861).
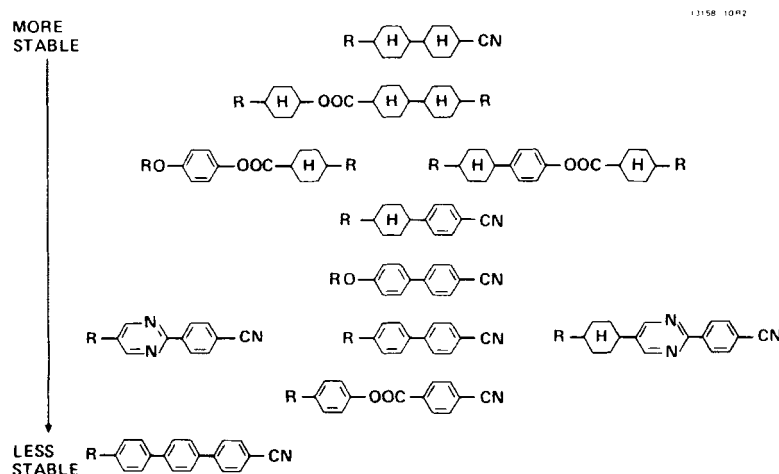

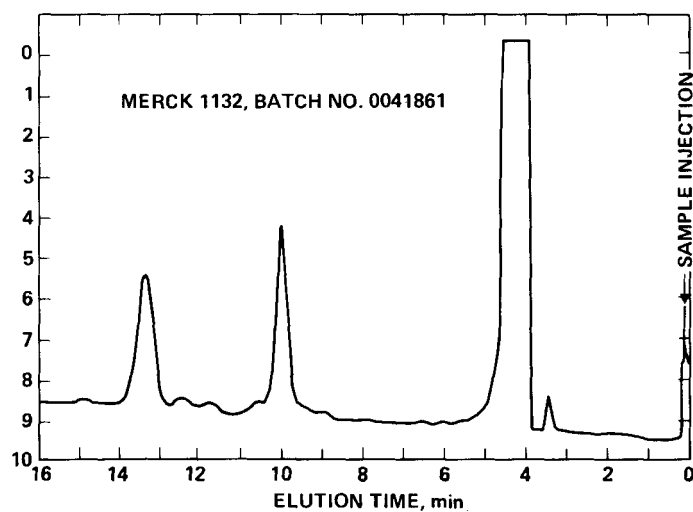FIGURE 11   Relative near-UV photostability of LC class structures.

13158-12

FIGURE 12   HPLC trace of impure Merck-1132[†] (batch 0041861).

The HPLC curve of Merck 1132 (batch 7945197) in Figure 7 showed only a small impurity peak preceding the component peak. The 0041861 batch (Figure 12) showed several impurities, particularly as two relatively large peaks (along with several smaller peaks) eluted after the component peak. Using height peak calculations, we estimated that these impurities totaled about 1.62% of the sample, which was an unacceptably high level.
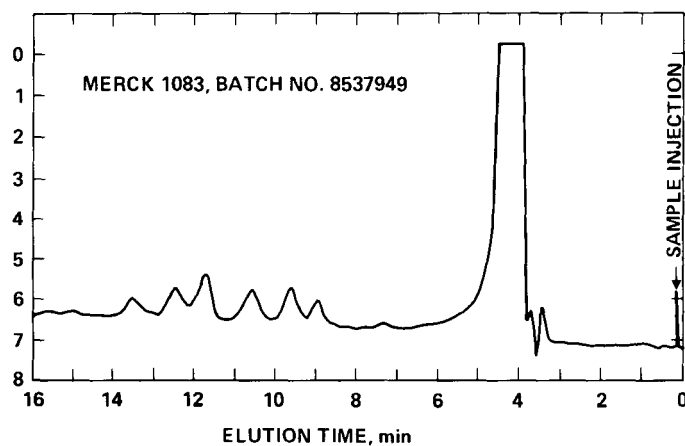
13158 13

FIGURE 13   HPLC trace of impure Merck-1083[†] (batch 8537949).

The major impurity peaks in Merck-1132,† (batch 0041861) after the cyanobiphenylcyclohexane (5YPPCN) had completely cleared the column, were considerable. This result, along with the Figure 12 result, indicates that the impurities are probably more polar than any of the components.

The Merck-1083† (batch 8537949) was analyzed, and its HPLC analysis showed a large group of impurities (Figure 13), three of which corresponded in position to the smaller impurity peaks observed in impure Merck-1132† (Figure 12). This batch of Merck-1083† was too impure to be included in our structure correlation studies, and the mixture showed a correspondingly low photostability value.

Results from GC analyses of Merck-1132 samples are shown in Figures 14 and 15. The 7945197 batch (Figure 14) showed only a small impurity shoulder after the three phenylcyclohexane components. The 0041861 batch of Merck-1132† (Figure 15) showed several major impurities both before and after the biphenylcyclohexane peak.

The impure 0041861 batch of Merck-1132† was purified by Prep-HPLC. A typical UV detection curve from the Prep column is shown in Figure 16, which also indicates the positions of the fractions which were separated. After fractions 2 and 3 (containing the four major components) were analyzed, they were combined. Fractions 5 and 6 correspond respectively, to the two major impurity peaks noted in Figure 12. The GC impurity analysis of fractions 2 and 3, (shown in Figure 17) indicated that the impurity peaks previously observed
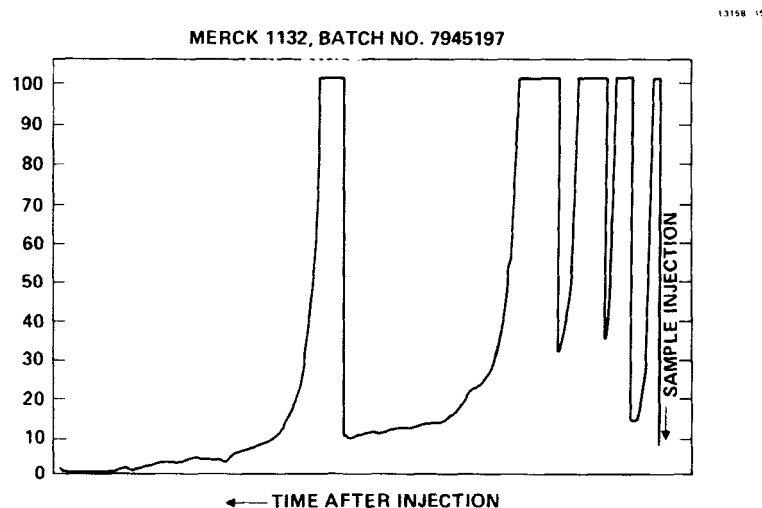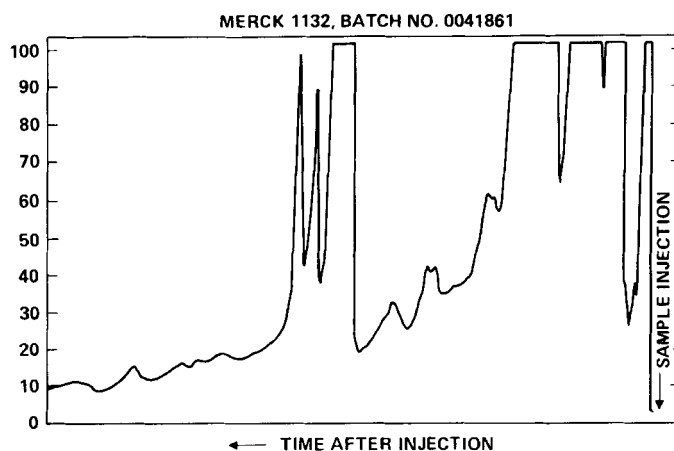

FIGURE 14   GC trace of Merck-1132 (batch 7945197).

MERCK 1132, BATCH NO. 0041861

FIGURE 15   GC trace of impure Merck-1132† (batch 0041861).

before purification (Figure 15) had been removed. Similarly, the analytical HPLC analysis (Figure 18) of fractions 2 and 3 show that impurities are absent.

However, the UV to visible absorbing impurities were either concentrated or generated by the Prep-HPLC purification of Merck-
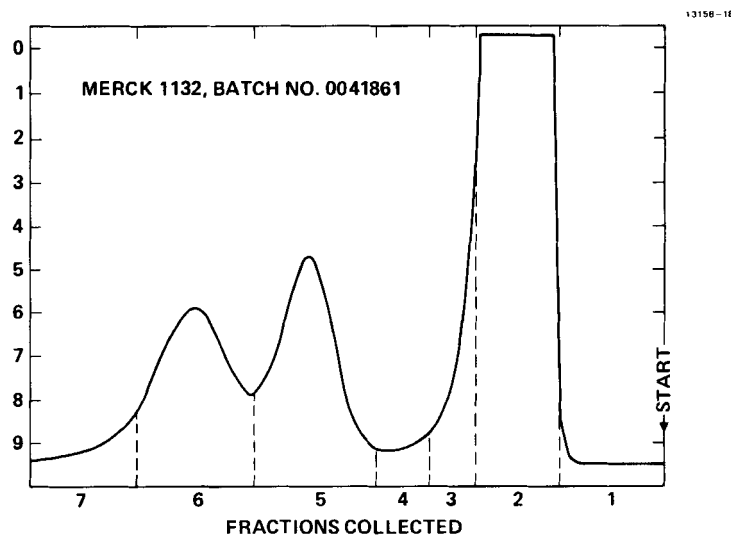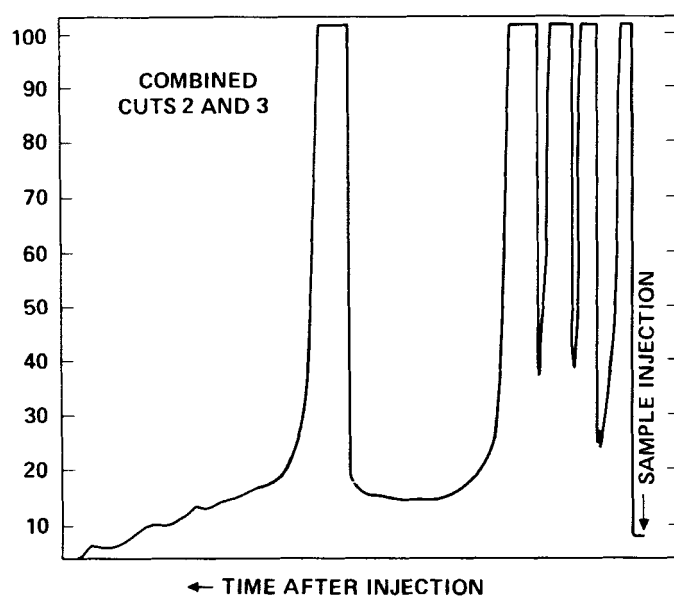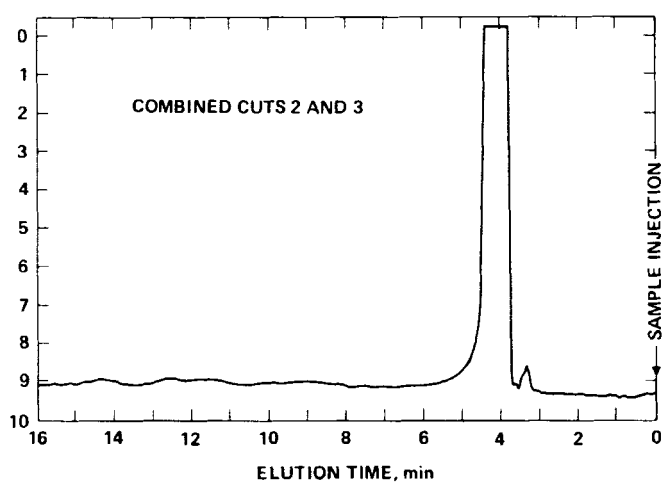
MERCK 1132, BATCH NO. 0041861

FRACTIONS COLLECTED

FIGURE 16   Typical UV detection curve from the purification of Merck-1132 (batch 0041861) by preparative HPLC.

FIGURE 17   GC trace of Merck-1132⁺ after purification by Prep-HPLC.

FIGURE 18   HPLC trace of Merck-1132⁺ after purification.

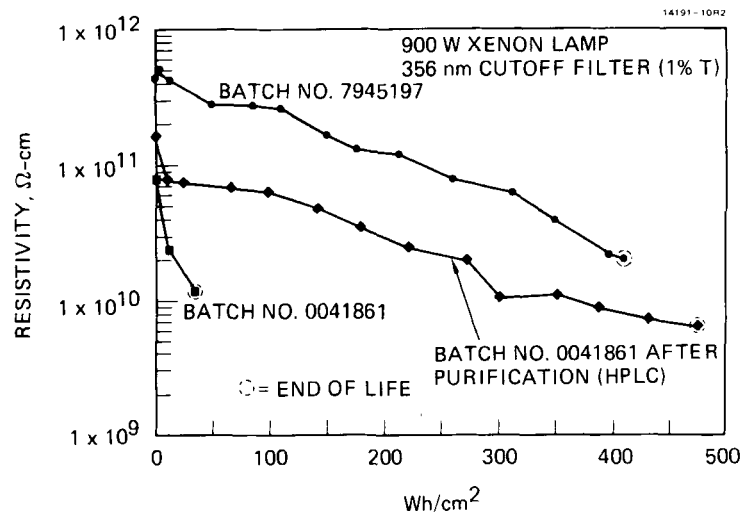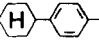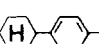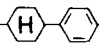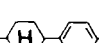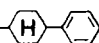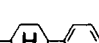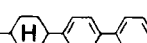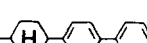FIGURE 19   Photostability of Merck-1132 LC mixtures.

1132†. It was important to study the photostability of the purified sample to determine whether the visible absorption impurities are more (or less) important than the impurities observed by GC and HPLC. The very short lifetime for the Merck-1132† batch 0041861, which contained about 1.62% impurity, was attributed to the presence of the polar impurities in the LC. After separating the four major components of the 1132 LC mixture from the impurities by Prep-HPLC, we found that the photostability was extended tenfold, as shown in Figure 19. From the initial lifetime of 35 Wh/cm^2 with the impure batch, we increased the photostability to 393 and 488 Wh/cm^2 in two test cells filled with the 1132 after Prep-HPLC purification. Initial GC and HPLC analyses of the two polar fractions (5 and 6 in Figure 16) that were isolated during the purification procedure showed the presence of numerous components within each fraction. Detailed analysis of fractions 5 and 6 were done on a Finnigan OWA GC/mass spectrometer equipped with a 30 m high resolution fused silica capillary SE-54 column. Tentative identification of isolated major components was based on the EI mass fragmentogram of each species. The results are shown in Table IV. The major impurities represent amides of the propyl- and pentyl-p-cyanophenylcyclohexane with one more unit of unsaturation. The amide impurity might have come from the synthesis step of the phenylcyclohexane components since amides are intermediates in the Friedel-Crafts acylation procedure reported by Eidenschink[2] for the phen-

TABLE IV

Merck-1132 impurities indentified by GC/MS from Prep-LC cuts 5 and 6 (batch 0041861)   16261—1

IMPURITIES	CUT NO. 5	CUT NO. 6
CHLOROOCTANE	✓	—
CHLORODECANE	✓	—
C_3H_7 —(H)—(◯)— CN *	✓	✓
C_3H_7 —(H)—(◯)— C(=O)—NH_2 *‡	✓	✓
C_5H_{11} —(H)—(◯)— CN *	✓	✓
C_5H_{11} —(H)—(◯)— C(=O)—NH_2 *‡	✓	✓
C_7H_{15} —(H)—(◯)— CN *	✓	✓
C_7H_{15} —(H)—(◯)— C(=O)—NH_2 *‡	✓	✓
C_5H_{11} —(H)—(◯)—(◯)— CN	✓	—
C_5H_{11} —(H)—(◯)—(◯)— CN *‡	✓	✓

*ONE MORE UNIT OF UNSATURATION
‡TWO PEAKS, ISOMERIC STRUCTURES

ylcyclohexane liquid crystal synthesis as shown in Figure 20. The presence of carbonyl and unsaturated impurities in the liquid crystal suggest photoinstability mechanisms similar to those previously found for BDH-E7 by Yamagishi, et al.[1]

To prove that the separated impurities were the limiting factor in the LC photostability, we doped a pure Merck-1132 mixture with 1% of fractions 5 and 6. Demountable test cells were fabricated with this doped LC and with pure Merck-1132 as a control. The reference cell showed a lifetime of 162 Wh/cm² versus 26, 29, and 32 Wh/cm² with
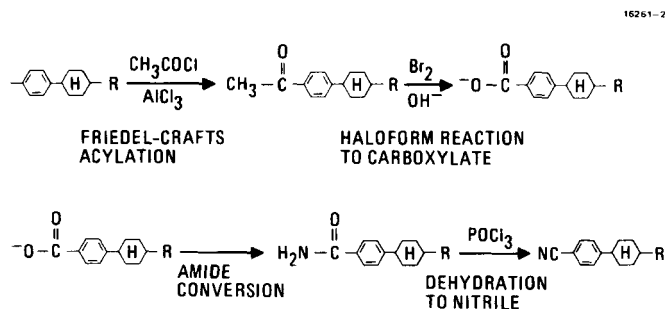
FIGURE 20   Phenylcyclohexane liquid crystal synthesis.

the doped Merck-1132, depending on handling techniques. This effect is shown in Figure 21. The fivefold decrease in the lifetime of the doped samples clearly indicates that these polar impurities are responsible for decreased photostability of the Merck-1132.
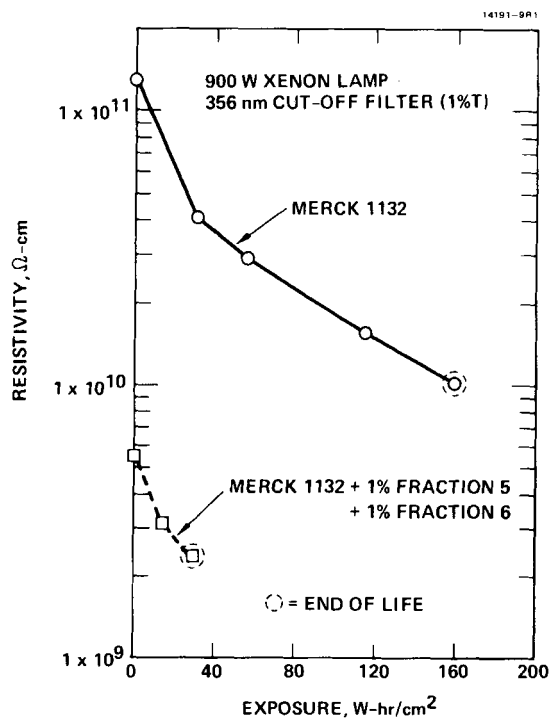

FIGURE 21   Exposure of pure and doped Merck-1132 in demountable test cells.

IV. CONCLUSIONS

The chemical structures of LC components have a strong effect on the UV/blue light photostability of mixtures used in LCLV cells. In general, components with more cyclohexane groups are more photostable (e.g., phenylcyclohexane instead of biphenyl, and phenylcyclohexanecarboxylate instead of phenylbenzoate).

The presence of small amounts of certain impurities (usually more polar structures than the parent LC) can sharply limit the photostability of a LC and offset the potential advantages of using components that are basically more stable when present without impurities.

Merck ZLI-1132 is much more stable than BDH-E7 in both the blue light and near UV regions. Merck ZLI-1800 LC was far more photostable than the others tested. Under accelerated tests (356 nm cutoff), it lasted four times longer than 1132. Although 1800 has a low birefringence, in test cells it showed satisfactory electro-optical response characteristics.

V. Acknowledgments

References

1. F. G. Yamagishi, D. S. Smythe, L. J. Miller and J. D. Margerum, *Liquid Crystal and Ordered Fluids*, Vol. 3, p. 475, J. F. Johnson and R. S. Porter, Eds. (Plenum Pub., 1978).
2. R. Eidenschink, D. Erdmann, J. Krause and L. Pohl, Angew. Chem., **89**, 103 (1977).